Eur. Phys. J. B **58**, 269–278 (2007)
DOI: 10.1140/epjb/e2007-00230-4

THE EUROPEAN PHYSICAL JOURNAL B

Slowly moving matter-wave gap soliton propagation in weak random optical lattices

M.R. Zhang[1,2], X.Y. Jiang[2,a], Y.L. Zhang[2], L. Shi[2], J. Zi[1], and J.Y. Zhou[3]

[1] Surface Physics Laboratory (National Key Lab), Fudan University, Shanghai 200433, P.R. China
[2] Institute of Microsystem and Information Technology, CAS, Shanghai 200050, P.R. China
[3] State Key Laboratory of Optoelectronic Materials and Technologies, Zhongshan University, Guangzhou 510275, P.R. China

Received 7 March 2007 / Received in final form 22 June 2007
Published online 8 September 2007 –

Abstract. We systematically investigate slowly moving matter-wave gap soliton propagation in weak random optical lattices. With the weak randomness, an effective-particle theory is constructed to show that the motion of a gap soliton is similar to a particle moving in random potentials. Based on the effective-particle theory, the effects of the randomness on gap solitons are obtained and the trajectories of gap solitons are well predicted. Moreover, the general laws that describe the movement depending on the weak randomness are obtained. We find that with an increase of the random strength, the ensemble-average velocity reduces slowly and the reflection probability becomes larger. The theoretical results based on the effective-particle theory are confirmed by the numerical simulations based on the Gross-Pitaevskii equation.

PACS. 03.75.Lm Tunneling, Josephson effect, Bose-Einstein condensates in periodic potentials, solitons, vortices, and topological excitations – 42.65.Tg Optical solitons; nonlinear guided waves – 05.45.Yv Solitons

1 Introduction

Bose-Einstein condensates (BECs) in periodic potentials are presently attracting considerable theoretical and experimental interests [1–6] due to the possibility to explore a fascinating wealth of physical phenomena ranging from Bloch oscillations [3], Landau-Zener tunnelling [4] to lensing effect [5]. In the mean-field approximation, these systems can be treated as nonlinear periodic systems, in which the periodic potentials are from the interference of laser beams and the nonlinearity comes from the interatomic interactions. In such nonlinear periodic systems, a very important excitation is the formation of gap solitons (GSs) [6]. The term of "gap soliton" was first proposed by Chen and Mills when they studied the light propagation in periodic Kerr materials [7]. They showed that the nonlinearity can lead to an optical pulse localization when the optical frequency lies in the gap. These localized wave packets are called GSs. After that, GSs have intensively been studied in optical systems and BEC systems [6,9–18]. Many theoretical methods, such as the coupled-mode method [10–12,15] and the multi-scale expansion method [13,14] are employed to study the evolution of GSs. All theoretical studies reveal that GSs are solitary waves which can propagate inside the nonlinear periodic systems *without deformation*. Recently, a direct experimental observation of matter wave GS in an ^{87}Rb BEC, containing about 250 atoms, has been reported [6].

The propagation of GSs in non-perfect lattices is another interesting topic. In optical systems, GS propagation in nonuniform Bragg lattices in which the lattice constants change continuously had been studied by Sterke et al. [8]. In their studies, the slow continuous change of lattice constants is treated as perturbations and the GS motion can be described by the effective particle picture (EPP). In the EPP, GSs can be treated as moving particles with effective forces acting on it. They also studied the effects of defects on the motion of GSs. But, so far, GS propagation in periodic potentials with weak *randomness* has not been studied.

In this paper, we investigate the propagation of slowly moving matter wave GSs in periodic potentials with weak randomness. Physically, the weak randomness could be caused by the fluctuation of optical lattices (generated by the laser beams). We focus on the BECs in shallow optical lattices. In this case, the matter wave GSs can be described by the coupled-mode theory [12,15]. Based on the previous studies [8,19–21], we introduce the EPP into this nonlinear random system. In this way, we find that the GS is acted upon by an effective force, and we proceed to give a detailed interpretation of the force. From this force, the effective potentials are as well-defined as to predict the GS trajectories. Moreover, from the EPP, the general laws of the GS movement depending on the weak

[a] e-mail: xyjiang@mail.sim.ac.cn

randomness are obtained, such as, although the change of the local velocity can be large with the increase of the random strength, the ensemble-average velocity reduces slowly, and the reduction is proportional to the variance of the randomness. In addition, the reflection probability becomes larger with the random strength. To confirm the theoretical studies based on the EPP, the GS motion is also simulated by the numerical finite-difference time-domain (FDTD) methods based on the GPEs [22]. After comparing with each other, we find that the theoretical results obtained from the EPP agree very well with the results from the direct numerical simulations.

The paper is constructed as follows: in Section 2, we introduce the setup of the system in detail. In Section 3, the EPP based on the coupled-mode theory is constructed, and the GS trajectories are obtained. In Section 4, we simulate the motion of GS by the numerical FDTD methods to confirm the validity of the EPP, and we get the general laws that describe the GS movement depending on the randomness. Finally, in Section 6, we summarize our results.

2 The setup of our model

Here we consider a BEC immersed in an optical lattice and a highly elongated harmonic trap. At low enough temperatures, the effect of the thermal Bose gas components can be neglected and the many-particles system of trapped atoms can be described by a macro wave function $\Psi(\mathbf{r},t)$. In the mean field approximation, the macro wave function obeys the three-dimensional (3D) GPE [23,24]

$$i\hbar\frac{\partial\Psi(\mathbf{r},t)}{\partial t}=\left[-\frac{\hbar^2\nabla^2}{2m}+V_{ext}(\mathbf{r})+g|\Psi(\mathbf{r},t)|^2\right]\Psi(\mathbf{r},t), \quad (1)$$

where $\hbar$ is Plank's constant, m is the atomic mass, $g=4\pi\hbar^2a_s/m$ is the nonlinear coefficient which accounts the mean field produced by other bosons, and a_s is the s-wave scattering length. In equation (1), the external potential $V_{ext}(\mathbf{r})$ which describes both the trap potential and the potential arising from the optical induced interference pattern, is given by:

$$V_{ext}(\mathbf{r})=E_l\sin\left(\frac{2\pi x}{L}\right)+\frac{1}{2}m[\omega_x^2x^2+\omega_\perp^2(y^2+z^2)]. \quad (2)$$

Here L is the lattice period, $E_l(x_i)$ is the depth of the optical potential at ith cell, and ω_x and $\omega_\perp$ denote the radial and longitudinal frequencies of the anisotropic trap ($\omega_x\ll\omega_\perp$), respectively.

In the 3D GPE (1), the potential can be decomposed as $V_{ext}(\mathbf{r})=V_x(x)+V_\perp(y,z)$ and the macro wave function can be expressed as $\Psi=\Psi_\perp(y,z)\Psi_x(x)$. Because the BEC is strongly confined in the y-z plane, the radial part of the macroscopic wave function $\Psi_\perp(y,z)$ approximately satisfies

$$\frac{\hbar^2}{2m}\nabla_\perp^2\Psi_\perp+\frac{1}{2}\omega_\perp^2\rho^2\Psi_\perp=E_\perp\Psi_\perp. \quad (3)$$

In equation (3), the first eigenfunction (zero-node) with the eigenvalue $E_\perp=\hbar\omega_\perp$ is

$$\Psi_\perp(y,z)=\sqrt{\frac{m\omega_\perp}{\pi\hbar}}\exp\left[-\frac{m\omega_\perp}{2\hbar}(y^2+z^2)\right]. \quad (4)$$

By integrating in the y-z plane, applying the transformation $\Psi_x\rightarrow\Psi_xe^{-i\omega_\perp t}$, and assuming the frequency of the trap (ω_x) is much smaller than the lattice frequency $2\pi/L$, we can obtain the one-dimensional GPE

$$i\hbar\frac{\partial\Psi_x(x,t)}{\partial t}=-\frac{\hbar^2}{2m}\frac{\partial^2\Psi_x(x,t)}{\partial x^2}+E_l\sin(\frac{2\pi x}{L})\Psi_x(x,t)+2a_s\hbar\omega_\perp|\Psi_x(x,t)|^2\Psi_x(x,t). \quad (5)$$

In this system, the weak spatial randomness of the optical lattice is included, this means the optical potential depths in different cells are different. And the potential depth of ith cell (i.e., $E_l(x_i)$) can be written as

$$E_l(x_i)=E_0(1+W\gamma_i), \quad (6)$$

where E_0 is the average potential depth, W is the strength of weak randomness, and γ_i is the random number to characterize the randomness. In this system, the random numbers γ_i are set to satisfy the Gaussian distribution

$$\rho(\gamma)=C_\gamma e^{-\gamma^2/\sigma_\gamma^2}, \quad (7)$$

where $\sigma_\gamma=1$ is the root mean square of Gaussian distribution, and $C_\gamma=1/\sqrt{\pi}$ is the normalization coefficient.

After introducing the dimensionless variables $t'=t/t_0$, $x'=x/x_0+\pi/2$, $\Psi_x=u/L_1^{1/2}$, and $V_l=E_l/E_r$ and choosing $x_0=L/2\pi$, $t_0=mx_0^2/\hbar$, $L_1=2\omega_\perp|a_s|mx_0^2/\hbar$ and $E_r=\hbar^2/mx_0^2$, equation (5) can be reduced to the following normalized one-dimensional GPE [26]

$$i\frac{\partial u}{\partial t}=-\frac{1}{2}\frac{\partial^2u}{\partial x^2}+V_l(x_i)\cos(x)u+\sigma|u|^2u, \quad (8)$$

where $\sigma=\mathtt{sgn}(a_s)$. Because the depth of optical lattice is very shallow, the condition $E_0/E_r=V_l^0\ll1$ is satisfied.

To study the motion of GSs in the weak random optical lattice, the setup of the system is shown in Figure 1. In region I, the optical lattice is perfectly periodic (i.e. $V_l(i)=V_0$), and a moving GS with velocity v_0 is generated as the incidence to region II. In region II, the weak randomness of the optical potential is introduced in (i.e. $V_l(i)=V_0(1+W\gamma_i)$), and the propagation of GSs is theoretically and numerically studied. The theoretical EPP description for the moving GS in the weak randomness system will be constructed. To confirm the results from the EPP, the GS motions are also numerically simulated by the FDTD method based on equation (8). Moreover, the general conclusions regrading the GS motion, i.e. the ensemble-average velocity and the reflection, are obtained. Because of the limitation of the computer resources in the numerical simulation, the length of the system is quite limited (about 25 times of the soliton width), so that we need about 20 configurations of the system to obtain the ensemble-average value.

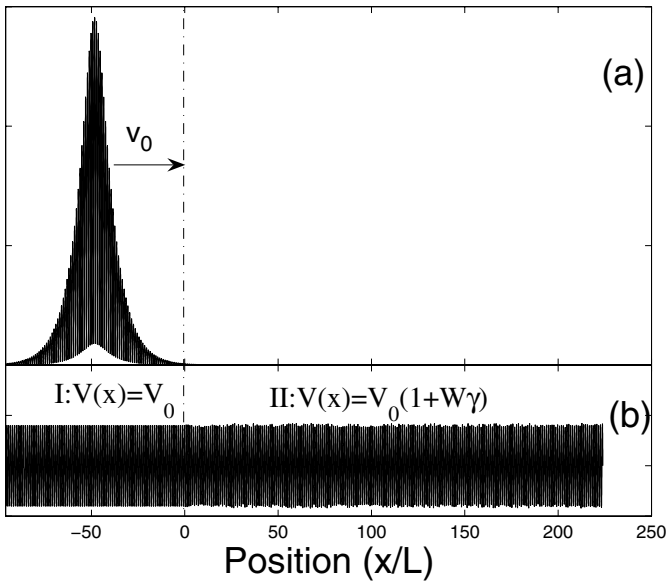

Fig. 1. Schematics shows the setup of our model. In region I, the optical lattice is perfect, while in region II, a weak randomness of the optical lattice is introduced. A moving GS with initial velocity v_0 is generated in region I and then incident to the region II.

3 The effective particle picture

In this section, we will construct the EPP for matter wave GSs in weak random systems based on the coupled-mode theory and derive the expression of the effective forces and the effective potentials.

Coupled mode theory is widely used to describe the matter waves in optical lattice (such as the BEC) very well when the optical potential is very shallow [15]. Here we give a brief description of the coupled-mode theory. First, we suppose there is no linear and the nonlinear potentials in equation (8), then matter waves with its chemical potential μ can be expressed as $u(z,t) = e^{-i\mu t}[u_f(x,t)e^{ikx} + u_b(x,t)e^{-ikx}]$ where $k = \sqrt{2\mu}$ is the wave vector and the constant u_f and u_b label the amplitude of the fields propagation forwards and backwards. The basic idea of the coupled-mode description is if the modulations are very small the solution has the same form only u_f and u_b vary slowly with z and t:

$$\left|\frac{\partial u_{f,b}}{\partial t}\right| \ll \mu\left|u_{f,b}\right|, \qquad \left|\frac{\partial u_{f,b}}{\partial z}\right| \ll k\left|u_{f,b}\right|. \tag{9}$$

For matter waves with the chemical potential (μ) near the Bragg condition at $\mu_B = k_B^2/2 = 0.125$ [25], the solution of equation (8) can be expressed as:

$$u(z,t) = e^{-i\mu t}[u_f(x,t)e^{ik_B x} + u_b(x,t)e^{-ik_B x}]. \tag{10}$$

Now inserting equation (10) into equation (8) and using the slowly varying conditions (9), we find that

$$\begin{aligned}\Bigg[\left(i\frac{\partial}{\partial t} + ik_B\frac{\partial}{\partial x} + \mu - \frac{1}{2}k_B^2\right)u_f(x,t) + \frac{V_l}{2}\left(u_b(x,t)\right) \\ + u_f e^{2ik_B x} - \sigma(|u_f|^2 + 2|u_b|^2)u_f\Bigg]e^{ik_B x} \\ + \Bigg[\left(i\frac{\partial}{\partial t} - ik_B\frac{\partial}{\partial x} + \mu - \frac{1}{2}k_B^2\right)u_b(x,t) \\ + \frac{V_l}{2}\left(u_f(x,t) + u_b e^{2ik_B x}\right) - \sigma(2|u_f|^2 \\ + |u_b|^2)u_b\Bigg]e^{-ik_B x} = 0.\end{aligned} \tag{11}$$

In equation (11), the remaining problematic terms are the terms involving $e^{\pm 2k_B x}$. Sterke et al. had shown that such components of higher spatial frequency would only couple back to $u_{f,b}$ involving terms of V_l^2 [9]. Since V_l is very small, such effects can be neglected. Therefore we can obtain the nonlinear coupled-mode equations (NLCMEs) from equation (11):

$$i\frac{\partial u_f}{\partial x} + \frac{i}{k_B}\frac{\partial u_f}{\partial t} + \Delta k u_f + \kappa(x)u_b + \alpha(|u_f|^2 + 2|u_b|^2)u_f = 0, \tag{12a}$$

$$-i\frac{\partial u_b}{\partial x} + \frac{i}{k_B}\frac{\partial u_b}{\partial t} + \Delta k u_b + \kappa(x)u_f + \alpha(2|u_f|^2 + |u_b|^2)u_b = 0, \tag{12b}$$

in which $\Delta k = (2\mu - k_B^2)/2k_B$ is the value to represent the difference between the energy μ and the gap center energy level, $\kappa(x) = V_l(x)/2k_B = \kappa_0(1 + W\gamma)$ is the local coupling coefficient from which the random potential is introduced into the coupled-mode theory, and $\alpha = -\sigma/k_B$ is the nonlinear coefficient.

In equation (8), if we suppose the perfect periodic potentials without randomness and nonlinearity, the NLCMEs reduce to two coupled linear equations. And the band gap structure can be obtained from the linear coupled-mode equations. In this case, the envelope functions have the form $u_{f,b} = v_{f,b}e^{iQx}$, and the constants $v_{f,b}$ satisfy the following equations:

$$\begin{bmatrix}\Delta k - Q & \kappa_0 \\ \kappa_0 & \Delta k + Q\end{bmatrix}\begin{bmatrix}v_f \\ v_b\end{bmatrix} = 0. \tag{13}$$

Then the dispersion relation can be expressed as:

$$\mu = \frac{k_B^2}{2} \pm k_B\sqrt{\kappa_0^2 + Q^2}. \tag{14}$$

From equation (14) we can see that the energy gap width is equal to $2k_B\kappa_0$. Because $2k_B\kappa_0 = V_l^0 \ll 1$, the energy gap of the periodic potential is very narrow.

In region I, the optical lattice is perfect ($\kappa(x) = \kappa_0 = V_0/2k_B$) and the GS solution can be obtained. For the GS in a perfect lattice, the amplitude of the forward and backward waves in equation (12) are [10,11]:

$$u_{f,b}(x,t) = A_{f,b}(x,t)e^{i\phi_{f,b}}\ , \tag{15}$$

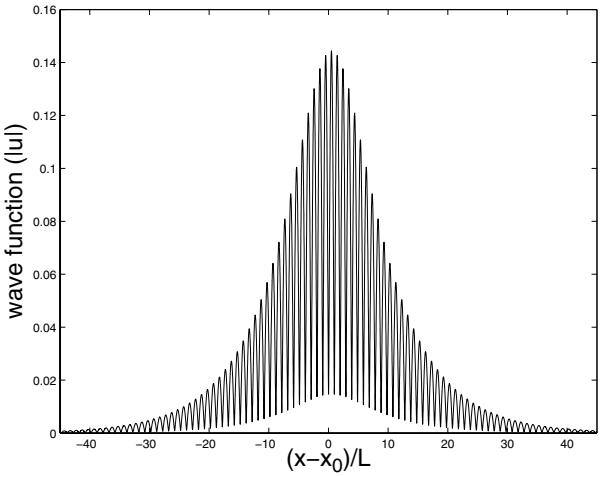

Fig. 2. Moving GS solution in a perfectly periodic optical lattice with the following parameters: chemical potential $\mu = 0.127$, optical potential $V_0 = 0.02$, nonlinear coefficient $\sigma = -1$, and the initial velocity $\beta_0 = 0.1325$. This figure shows that the spatial distribution of GS ($u(x)$) is laterally symmetric in space.

where

$$A_f = \left(\frac{\kappa_0}{|\alpha|}\frac{2(1+\beta)\sqrt{1-\beta^2}}{3-\beta^2}\frac{\cos^2\theta}{\sin(\theta)+\cosh[2y]}\right)^{1/2}, \tag{16a}$$

$$A_b = \left(\frac{\kappa_0}{|\alpha|}\frac{2(1-\beta)\sqrt{1-\beta^2}}{3-\beta^2}\frac{\cos^2\theta}{\sin(\theta)+\cosh[2y]}\right)^{1/2}, \tag{16b}$$

$$\phi_f = \phi_0 + \left(\frac{4\beta}{3-\beta^2}+1\right)\arctan\left(\frac{\cos\theta}{1+\sin\theta}\tanh[y]\right) + (\beta\tan\theta)y - \frac{\pi}{2}, \tag{16c}$$

$$\phi_b = \phi_0 + \left(\frac{4\beta}{3-\beta^2}-1\right)\arctan\left(\frac{\cos\theta}{1+\sin\theta}\tanh[y]\right) + (\beta\tan\theta)y + \frac{\pi}{2}. \tag{16d}$$

Here $\beta = v/k_B$ is the GS normalized velocity and v is the velocity which is a free parameter of the strict GS solution, $\theta = \arcsin\frac{\Delta k}{\kappa_0\sqrt{1-\beta^2}}$, and $y = \frac{\kappa_0\cos\theta}{\sqrt{1-\beta^2}}(x - x_0 - vt)$ are the GS moving coordinates and x_0 is the central position of the GS. The spatial distribution of a strict moving GS solution is shown in Figure 2, and we can see that it is lateral symmetric in space.

In region II, where the randomness is introduced, the strict GS solution does not exist. However, because the randomness is very weak based on the perturbation theory we can construct the EPP. In the EPP, the matter wave field can be assumed to keep as a GS during the motion. This is true as long as the radiative emission of matter wave GS can be neglected. In this assumption, the strict GS solutions are still available in region II. In addition, from the strict GS solutions (Eqs. (15) and (16)), we can see that the time-dependent parameters β and θ are able to fully characterize the GS. Therefore we are interested in the time evolution of β and θ. Our aim is to obtain the evolution equations of β and θ. Similar to the previous research in references [8,27], the EPP can be constructed by defining a set of moments which can completely characterize the GS. The moments, which are analogous to those used in references [8,27] are given below:

the total particle number Q

$$Q \equiv \int_{-\infty}^{+\infty}(|u_f|^2 + |u_b|^2)dx = \frac{4}{\alpha}\frac{1-\beta^2}{3-\beta^2}\left(\frac{\pi}{2}-\theta\right), \tag{17a}$$

the effective position x_s

$$x_s \equiv \frac{1}{Q}\int_{-\infty}^{+\infty} x(|u_f|^2 + |u_b|^2)dx = x_0 + vt, \tag{17b}$$

the effective velocity v_s

$$v_s \equiv \frac{1}{Q}\int_{-\infty}^{+\infty}(|u_f|^2 - |u_b|^2)dx = v, \tag{17c}$$

and the effective momentum P

$$\begin{aligned} P &\equiv \int_{-\infty}^{+\infty}\mathrm{Im}[u_f^*\partial_x u_f + u_b^*\partial_x u_b]dx \\ &= \frac{\kappa_0}{\alpha}\frac{4\beta\sqrt{1-\beta^2}}{3-\beta^2}\cos\theta \\ &\quad + \frac{\kappa_0}{\alpha}\frac{16\beta\sqrt{1-\beta^2}}{(3-\beta^2)^2}\left[\cos\theta - \sin\theta\left(\frac{\pi}{2}-\theta\right)\right]. \end{aligned} \tag{17d}$$

In these equations, "$\equiv$" represents the definition of these moments and "$=$" denotes the moments are which evaluated for the strict GS solutions. From equation (17), we can see that both the "particle number" Q and the momentum P are conserved quantities for a GS in perfect lattices.

Using the definition of the moments in equation (17) and the NLCMEs (12), time derivatives of the particle number (Q), effective momentum (P) and effective position (x_s) can be easily calculated:

$$\frac{dQ}{dt} = 0, \tag{18a}$$

$$\begin{aligned} F = \frac{dP}{dt} &= \kappa_0 W\int_{-\infty}^{+\infty}\left[\mathrm{Re}(2u_f u_b^*)\frac{\Delta\gamma}{\Delta x}\right]dx \\ &= -\kappa_0 W\int_{-\infty}^{+\infty}\frac{\partial[\mathrm{Re}(2u_f u_b^*)]}{\partial x}\gamma dx, \end{aligned} \tag{18b}$$

$$\frac{dx_s}{dt} = \frac{1}{Q}\int_{-\infty}^{+\infty}(|u_f|^2 - |u_b|^2)dx = v_s. \tag{18c}$$

Here, equation (18a) represents that the particle number is still conserved, while equation (18b) represents that the

momentum conservation is broken by the "force". Equation (18c) confirms that the definition of the effective position and the effective velocity given by equations (17b) and (17c) are *mutually consistent*. To solve the force F in equation (18b), $u_{f,b}$ must be known at all times, which include the full NLCMEs. Instead, as mentioned above, we assume that the moving GS is the same as a strict GS solution except for the time-dependent parameters. Furthermore, from the conservation of the particle number (18a), $\theta(t)$ can be expressed in terms of the normalized velocity $\beta(t)$ and the initial particle number Q_0

$$\theta(t) = \frac{\pi}{2} - \frac{\alpha}{4}\frac{3-\beta^2}{1-\beta^2}Q_0. \tag{19}$$

Since we only focus on the slowly moving case in this paper, the β^2-order terms can be neglected. The parameter θ in equation (19) can then be thought of time-independent (velocity-independent), and the momentum P in equation (17d) can then be approximated by:

$$P = \frac{\kappa_0}{\alpha}\left[\frac{4}{3}\cos\theta + \frac{16}{9}\Big(\cos\theta - \sin\theta\left(\frac{\pi}{2}-\theta\right)\Big)\right]\beta \equiv m_s\beta. \tag{20}$$

Note that if θ enters equation (20) as a velocity-independent parameter, the parameter m_s is velocity-independent too. Thus m_s in equation (20) can be treated as the *mass*, which is an intrinsic parameter of the GS. Using the above approximation, the EPP can be simplified as:

$$\frac{dx_s}{dt} = \beta k_B \ , \tag{21a}$$

$$F = \frac{dP}{dt}, \tag{21b}$$

$$P = m_s\beta. \tag{21c}$$

From equation (21b), we can obtain the motion details of a GS in a random system. In equation (21b), the "force" on a GS can be solved by evaluating the integrals in equation (18b). In the low-velocity limit, the change of the function $\mathrm{Re}(u_f u_b^*)$ is of β^2-order too, so that the force F only depends on the position of the GS. In other words, the force on the GS is a conservative one, and we can define the effective potential later.

To obtain the GS motion, the force in equation (21b) should be solved first. After introducing the "force-responding" function $g(x-x_s) = -\partial_x(2A_fA_b\cos(\phi_f - \phi_b))$ [28], equation (18b) can be simplified as

$$F(x_s) = \kappa_0 W\int_{-\infty}^{+\infty} g(x)\gamma(x)dx. \tag{22}$$

Obviously, the "force-responding" function $g(x-x_s)$ is independent of the randomness. The spatial distribution of the function $g(x-x_s)$ of a case is plotted in Figure 3. From this figure, we can see that the function is odd: $g(x_s+x) = -g(x_s-x)$ (the odd property can be obviously derived from the strict GS solution too), and when $x-x_s \to \pm\infty$, $g(x-x_s)\to 0$. To simplify the calculation, we can define a cutoff length x_{cut}, and suppose $g(x-x_s)\sim 0$ when $|x-x_s| > x_{cut}$. After that, the effective force can be approximated as

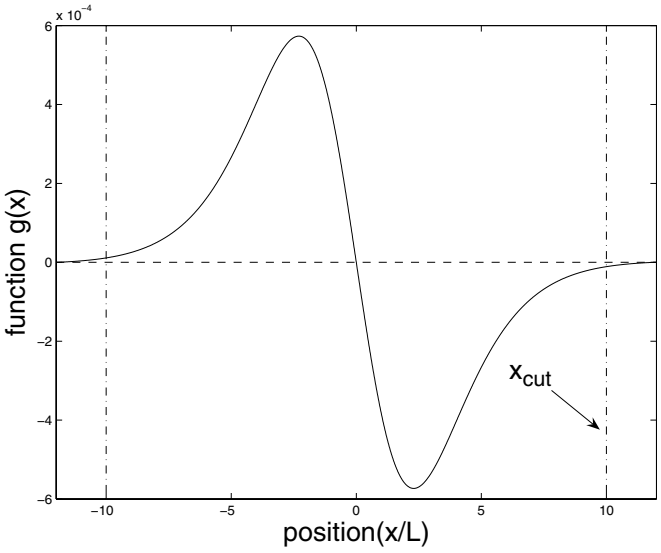

Fig. 3. The spatial distribution of the "force-responding" function $g(x-x_s)$. The parameters of the GS is same as the parameters in Figure 2. We can see that the function $g(x-x_s)$ is odd ($g(x_s+x) = -g(x_s-x)$) and when $(x-x_s)\to\pm\infty$, $g(x)\to 0$.

$$F(x_s) = \kappa_0 W\int_{x_s}^{x_s+x_{cut}} g(x-x_s)\gamma(x)dx + \kappa_0 W\int_{x_s-x_{cut}}^{x_s} g(x-x_s)\gamma(x)dx = F_f(x_s) + F_b(x_s). \tag{23}$$

Because $g(x-x_s)$ is odd, the force effects of the randomness on the GS front part and the back part are different. Such as when $\gamma(x) > 0$ (a positive random fluctuation), if the position x is at the GS front part ($x > x_s$), its contribution to the total force is negative (backward force), but if the position x is at the back part ($x < x_s$), its contribution is positive (forward force). Thus the force in equation (23) can be separated into two parts: $F_f(x_s) = \kappa_0 W\int_{x_s}^{x_s+x_{cut}} g(x-x_s)\gamma(x)dx$ is the "front-part" which is an integral over all contributions of the local fluctuation in the region of the GS front part, $F_b(x_s) = \kappa_0 W\int_{x_s-x_{cut}}^{x_s} g(x-x_s)\gamma(x)dx$ is the "back-part", which is the same of the back-part region. Equation (23) gives a more detailed interpretation of the origin of the force from the oddness property of the force-responding function.

Because the force is a conservative one, an effective potential on a GS can be defined:

$$U(x_s) = -\int_{x_0}^{x_s} F(x')dx' \tag{24}$$

where x_0 and x_s are the GS initial position and current position, respectively. The force in equation (24) can be discretized as

$$F(x') = \sum_{j=-n_{cut}}^{j=n_{cut}} \lambda_j \gamma_j \tag{25}$$

where the coefficients $\lambda_j = \kappa_0 W \int_{(j-1)L}^{jL} g(x-x')dx$. Substituting equation (25) into equation (24), the effective potential at x_s can be written as

$$U(x_s) = -\kappa_0 LW[\sum_{j=0}^{n_{cut}} (\gamma_{n_s-j} + \gamma_{n_s+j}) \int_{jL}^{n_{cut}L} dx g(x_s+x) - \sum_{j=0}^{n_{cut}} (\gamma_{n_0-j} + \gamma_{n_0+j}) \int_{jL}^{n_{cut}L} dx g(x_0+x)], \tag{26}$$

where $n_s = x_s/L$, $n_{cut} = x_{cut}/L$, and $n_0 = x_0/L$. In equation (26), the effective potential only depends on the random configurations near the GS initial position (x_0) and its current position (x_s). This is a general property for conservative potentials, whose value is determined by local conditions and independent of the dynamical process. It will also be shown that the integral in equation (24) over the evolution process should be cancelled with each other. The cancellation can be easily explained by the oddness property of the force-responding function $g(x)$. For example, we suppose at x_1 the $\gamma(x = x_1) > 0$, when the GS front-part passes the x_1, the contribution of this point to the integral of equation (24) is negative, but when the back-part passes through x_1, the contribution of this point to the integral is positive, which can exactly cancel the contribution at the front-part. To calculate the potential more concisely, we introduce the weight functions:

$$R(\gamma_{n_s \pm j}) = -\int_{jL}^{n_{cut}L} dx g(x_s+x). \tag{27}$$

Then, the effective potential can be calculated by the discrete summation:

$$U(x_s) = \kappa_0 LW \sum_{j=-n_{cut}}^{n_{cut}} R(\gamma_{n_s+j})\gamma_{n_s+j}. \tag{28}$$

The physical meaning of the weight function can be explained as the contribution of those points, whose position is in the range $|x - x_s| < x_{cut}$ to the effective potential. Because the GS has not passed through those points (or those points are still in GS range), their contribution to the effective potential is not zero. Similarly, to $g(x)$, the weight function R only depends on the GS field distribution and can be thought of as an integrated-contribution factor of the local fluctuation at x, when the GS is passing this point. The spatial distribution of the weight function $R(\gamma_{n_s+j})$ normalized by $R(\gamma_{n_s})$ of one case is plotted in Figure 4. From this figure, we can see that the weight function is even (the even property can also be obtained from Eq. (27)).

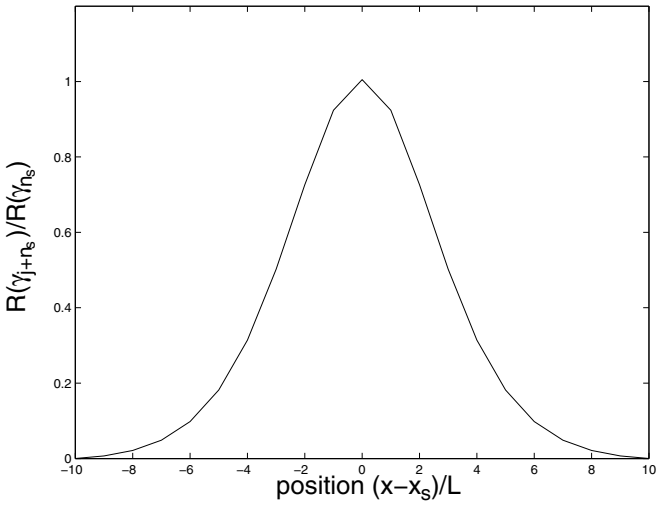

Fig. 4. The weight function $R(\gamma_{n_s+j})$ is normalized by $R(\gamma_{n_s})$ via the position. The parameters of the GS is the same as those used in Figure 2 and the value of $R(\gamma_{n_s}) = 0.0158$. We can see that the weight function is even.

After the effective potential is obtained, the equation of the mechanics-energy conservation based on the EPP can be written as:

$$\frac{m_s}{2}\beta^2(x) + U(x) = \frac{m_s}{2}\beta_0^2 + U(x_0). \tag{29}$$

Here β_0 is the initial normalized velocity and $\frac{m_s\beta^2(x)}{2}$ is the EPP "kinetic energy" of the GS at position x. From equations (28) and (29), we can see that if the random configurations are known, the GS trajectories can be obtained. We can set the effective potential of perfect lattice is zero ($U(x_0) = 0$), then from the conservation of equation (29), there exist a critical potential value:

$$U_c = \frac{m_s\beta_0^2}{2}. \tag{30}$$

If the effective potential is smaller than the critical potential, GSs can pass forwards. But if the local effective potential is larger than the critical potential ($U(x) > U_c$), GSs will be reflected.

4 GS propagation in weak random optical lattices

In the last section, the EPP is formally constructed. Based on the EPP, the GS trajectories can be obtained. The GS trajectories can also be obtained by the direct numerical FDTD simulations based on the GPE. In this section, to

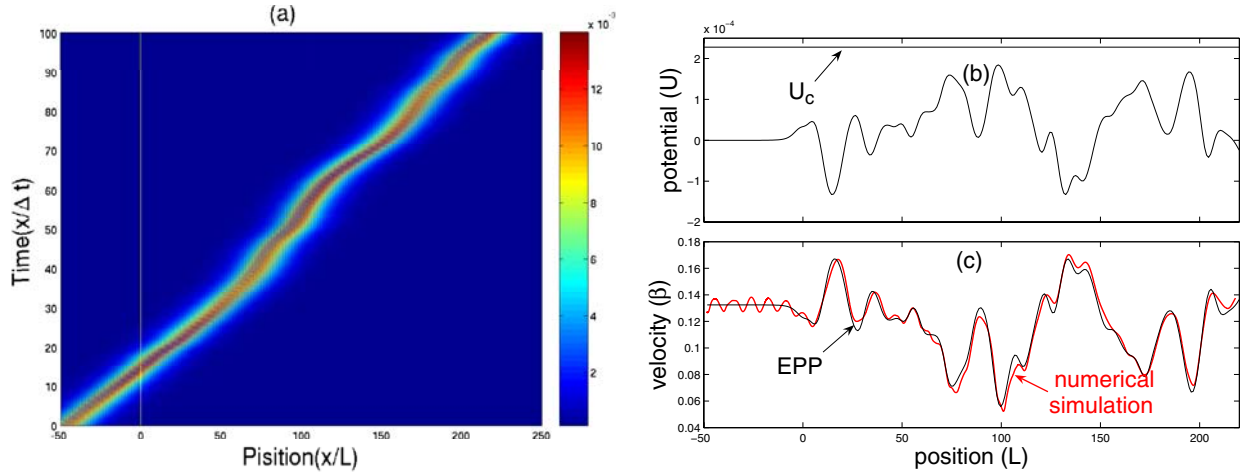

Fig. 5. (Color online) A GS passes forward in a weak random optical lattice. The time step is $\Delta t = 600$. The parameters of the GS are: chemical potential $\mu = 0.127$, optical potential $V_0 = 0.02$, nonlinear coefficient $c = -1$, the initial normalized-velocity $\beta_0 = 0.1325$, and the mass of the GS is $m_s = 2.561$. The random strength of the optical lattice $W = 0.035$. Figure (a) shows the evolution of GS calculated by the numerical FDTD simulations based on equation (8). Figure (b) shows the effective potential versus the position. During the propagation, the effective potentials are always smaller than the critical potential $U_c = 0.000224$. Figure (c) plots the trajectories in the $(\beta - x)$ plane. The trajectory solved from the EPP (black line) coincides with the trajectory obtained by the numerical FDTD simulations (red line).

confirm the validity of the EPP, the results of the numerical FDTD method based on the GPE (8) are compared with the EPP results. Eventually, the general laws of the GS movement in weak random optical lattices are discussed.

4.1 Numerical methods and the validity of the EPP

The numerical FDTD method of solving GPE (8) are briefly introduced at here. In the numerical simulation, the GPE (8) with the perfectly matched layer [22] is discretized via the Crank-Nicholson algorithm and solved by the FDTD methods. In the calculations 100 grid points per one lattice cell have been used, which results in the grid spacing being much smaller than the length of the GS. The computational domain extends over 500 lattice sites (about 25 times of the GS width). To keep numerical stability, a time grid $\delta t \sim 10^{-3}$ has been selected. In the following, the GS propagation in two random configurations, one corresponding to the passing forward case and the other corresponding to the reflected case, are simulated.

Corresponding to the passing forward case, time evolution of the GS (i.e, the GS position versus time) is plotted in Figure 5a which shows that the GS passes forward. This is in accordance with the potentials displayed in Figure 5b which shows that the effective potential is always smaller than the critical potential U_c. Moreover, to test the validity of EPP, the trajectories calculated by the EPP (black) with the trajectory obtained from the numerical FDTD simulations (red) are shown in Figure 5c. We find that they coincide with each other.

Similar to the passing forward case, for the reflected case, the GS evolution is shown in Figure 6a. From this figure, we can see that the GS is reflected at position $x_R \sim 140L$. This agrees with the results shown in Figure 6b: the effective potentials in region III are larger than the critical potential U_c. Finally, the GS trajectories obtained by two methods are plotted in Figure 6c. From this figure, we can see that they agree with each other very well.

From the two examples above, we can see that the theoretical results calculated using the EPP agree with the results from the numerical FDTD simulation very well. This confirms that the EPP is a valid method to describe the GS propagation in the periodic potential with weak randomness.

4.2 General laws of the GS movement depends on weak randomness

From the above analysis, we can see that the GS trajectories strongly depend on the local random configurations. In this subsection, we will obtain the general laws of the GS motion depending on the weak randomness.

To be consistent with the discussion in Section 3, the normalized ensemble-average velocity $\overline{\beta}$ (in the following this will also be called ensemble-average velocity) is used to characterize the GS movement. The ensemble-average velocity $(\overline{\beta})$ is defined as

$$\overline{\beta} = \frac{1}{k_B} \lim_{N\to\infty} \frac{NL}{\sum_i \Delta t_i}. \tag{31}$$

In equation (31) $\Delta t_i = L/v_i$ is the time in which the GS passes through the ith cell, and $v_i = \beta_i k_B$ is the velocity with which the GS passes through the ith cell. From

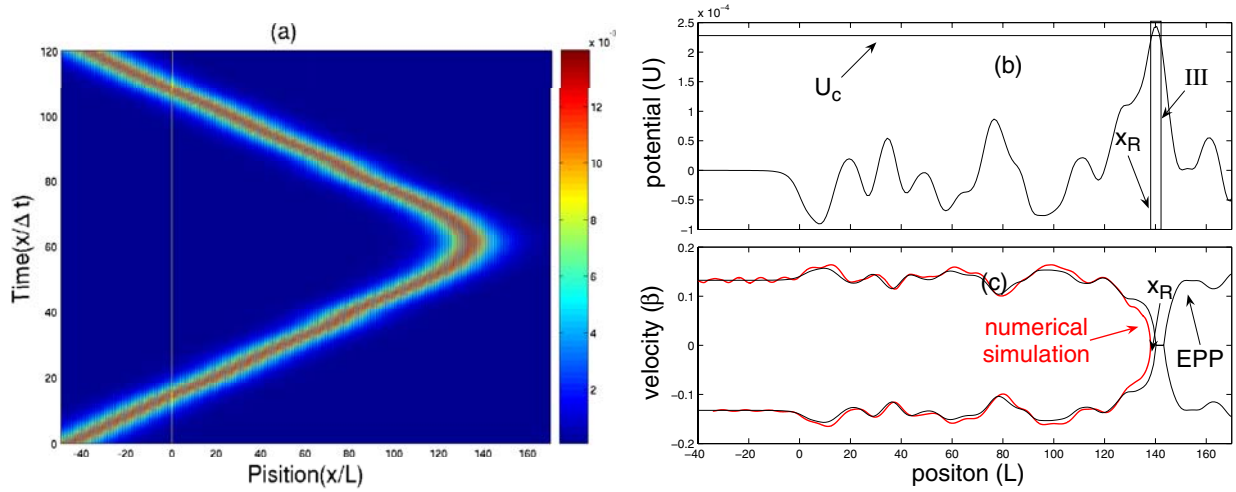

Fig. 6. (Color online) A GS is reflected in a weakly fluctuating optical lattice. The time step Δt and the parameter of GS are same to Figure 5, and the random strength is $W = 0.045$. Figure (a) shows time evolution of a GS in the optical lattice calculated by the numerical FDTD simulation. Figure (b) shows the effective potentials versus the position. We can see that in region III, the effective potentials are larger the critical value $U_c = 0.000224$. Figure (c) plots the trajectories in the $(\beta - x)$ plane. The trajectory obtained by the EPP (black line) and the FDTD simulations (red line) are agreeable with each other. At position x_R, where the effective potential is larger than the critical potential, the GS is reflected.

equation (29), we find that the time Δt_i in equation (31) is

$$\Delta t_i = \frac{L}{\beta_i k_B} = \frac{L}{k_B} \frac{1}{\sqrt{\beta_0^2 - \frac{2}{m_s} U_i}}. \tag{32}$$

From equation (26), we find that the effective potential U_i in equation (32) can be written as $U_i = C_u W \gamma_u^i$, in which $C_u = \kappa_0 g_0 L$ is the coefficient and $\gamma_u^i = \sum_{j=-n_{cut}}^{j=n_{cut}} \eta_j \gamma_{n_i+j}$ is the random number which characterizes the effective potential. Here, $g_0 = \sum_j R(\gamma_{n_i+j}) = -2\sum_j [\int_{jL}^{n_{cut}L} dx g(x_i + x)]$ and $\eta_j = R(\gamma_{n_i+j})/g_0$. Substituting equation (32) into equation (31) and transforming the discrete equation (31) into integral forms, the ensemble-average velocity can be written as:

$$\overline{\beta} = \frac{1}{\int d\gamma_u \frac{1}{\sqrt{\beta_0^2 - \frac{2C_u W \gamma_u}{m_s}}} \rho(\gamma_u)}, \tag{33}$$

where

$$\rho(\gamma_u) = C_{\gamma_u} e^{-\gamma_u^2/\sigma_{\gamma_u}^2}, \tag{34}$$

is the distribution of the random number γ_u [29]. In equation (34) $\sigma_{\gamma_u} = 1/[\sqrt{\sum_i \eta_i^2}]$ is the root mean square of the Gaussian distribution, and $C_{\gamma_u} = 1/[\sigma_{\gamma_u}\sqrt{\pi}]$ is the normalization coefficient.

Substitute equation (34) into equation (33), the ensemble-average velocity can be solved [30]. In addition, the ensemble-average velocity can also be obtained by the numerical FDTD simulations. In the numerical simulations, GSs propagate through about 5000 lattice sites which include about 20 configurations. The ensemble-average velocity $(\overline{\beta})$ versus the random strength (W) are plotted in Figure 7. From this figure, we can see that the

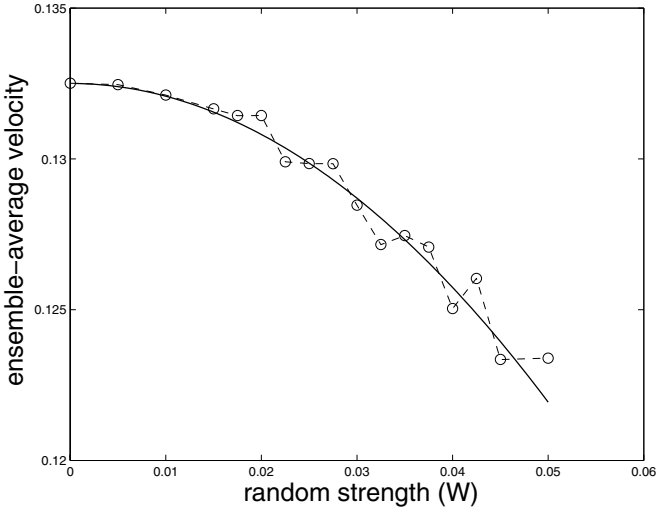

Fig. 7. The ensemble-average velocity of the GS $\overline{\beta}$ versus the random strength W. The initial parameters of the GS are same to the parameters in Figure 5. In this case, the coefficients in equation (33) are obtained: $C_u = 2.793$, $\sigma_{\gamma_u} = 0.297$ and $C_{\gamma_u} = 1.899$. The ensemble-average velocity $\overline{\beta}$ depending on the random strength calculated by the EPP (solid) and the numerical simulation (dash-dot line) agree with each other very well. From this figure, we can see that with the increase of the random strength, the ensemble-average velocity reduces slowly.

ensemble-average velocity calculated by the EPP (solid line) coincides with the one obtained from the numerical FDTD simulation (dot-dash line). This also proves that the EPP can describe the GS movement in a weak random system very well. Furthermore, from this figure we can see that with an increase of the random strength, the

ensemble-average velocity reduces slowly and the $\overline{\beta} - W$ relation is parabolic.

The small reduction of the ensemble-average velocity can be explained qualitatively from equations (31) and (32). Because the random strength is very small in our model, the probability that the effective potential is larger than the critical potential is very small. In the following, we only focus on the case that the effective potential is smaller than the critical potential. In this approximation, the local velocity in equation (29) can be expanded as

$$\beta_i = \beta_0 \left[1 - \frac{U_i}{m_s \beta_0^2} - \frac{1}{2} \left(\frac{U_i}{m_s \beta_0^2} \right)^2 - \cdots \right]. \quad (35)$$

Then the ensemble-average velocity in equation (33) can then be approximated with:

$$\overline{\beta} = \frac{\beta_0}{1 + \frac{C_u W}{m_s \beta_0^2} \overline{\gamma_u} + \frac{3}{2} (\frac{C_u W}{m_s \beta_0^2})^2 \overline{(\gamma_u)^2}}. \quad (36)$$

In equation (36), the average value $\overline{\gamma_u}$ is zero, and the value $\overline{\gamma_u^2}$ is a positive constant. The ensemble-average velocity can then be written as:

$$\overline{\beta} = \beta_0 \left[1 - \frac{3}{2} \left(\frac{C_u}{m_s \beta_0^2} \right)^2 W^2 \overline{(\gamma_u)^2} \right]. \quad (37)$$

In equation (35), the change of the local velocity is mainly from the first order term (i.e, $\beta_0 U_i/(m_s \beta_0^2)$) which can be close to β_0, while the reduction of the ensemble-average velocity in equation (37) is proportional to the second-order term, which is very small in this system. This means that although the change of the local velocity can be large, the reduction of the ensemble-average velocity is very small. Also from equation (37), we can see that the $\overline{\beta} - W$ relation is parabolic. Moreover, from equation (37), the reduction of the ensemble-average velocity is proportional to the value $\Gamma = W^2 \overline{\gamma_u^2}$. Using equation (34), the value (Γ) can be written as $\Gamma = (W^2 \overline{\gamma^2})/\sigma_{\gamma_u}^2$, in which $W^2 \overline{\gamma^2}$ is the variance of the weak randomness of optical lattices. Therefore, the reduction is proportional to the variance of the weak randomness.

Finally, the reflection probability depending on the random strength is solved. The condition of the reflected case can be solved from equation (30): when $C_u W \gamma_u > m_s \beta_0^2/2$, the GS will be reflected. Then, the critical value of the random number is $\gamma_u^c = m_s \beta_0^2/(2 C_u W)$, and the reflection probability is

$$P_r = \int_{\gamma_u^c}^{+\infty} \rho(\gamma_u) d\gamma_u. \quad (38)$$

The reflection probability P_r versus the random strength W is plotted in Figure 8. From this figure, we can see that with an increase of the random strength, the reflection probability becomes larger. This is because with an increase of the random strength, the probability that the effective potential is larger than the critical potential becomes larger.

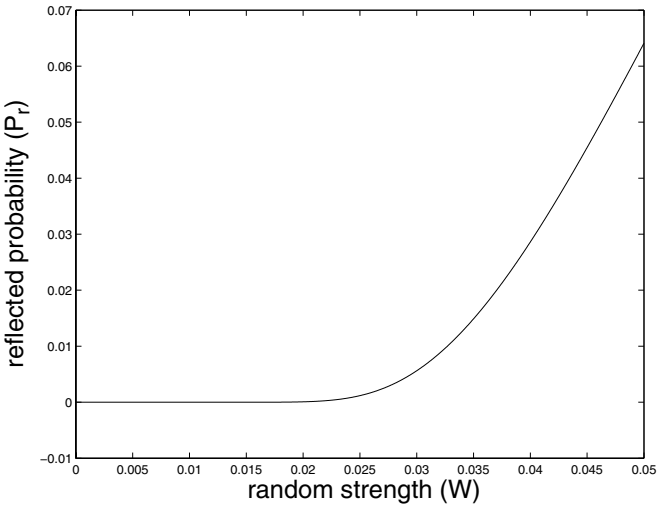

Fig. 8. The reflected probability P_r versus the random strength W. The parameters of the GS are same with the parameters in Figure 5. This figure shows that with the increase of the random strength W, the reflected probability P_r becomes larger.

5 Summary

In conclusion, slowly moving matter-wave GSs propagation in weak random optical lattices has been investigated in this paper. Introducing weak randomness, an EPP is constructed to describe the GS movement. From the EPP, we find that the GS behaves like a particle with conservative forces acting on it. Based on the conservative forces, the effective potentials are sufficiently well defined to obtain the GS trajectories. The detailed interpretations of the effective forces are found and the expressions for the effective potentials are obtained. Moreover, the general laws of the GS movement depending on the weak randomness are obtained. We find that although with the increase of random strength, the change of the local velocity can be large the reduction of the ensemble-average velocity is very small and proportional to the variance of the weak randomness. In addition, the reflection probability becomes larger along with the random strength. The theoretical results obtained by the EPP are confirmed by the numerical FDTD simulations based on the GPE.

This work has been supported by the NNSFC (Grant No. 10374096), SFMSBRP (Grant No. 2001CCA02800), the CAS-BaiRen program, and the Pujiang Talent Project (No. 05PJ14109).

References

1. A. Minguzzi, S. Succi, F. Toschi, M.P. Tosi, P. Vignolo, Phys. Rep. **395**, 223 (2004)
2. O. Morsch, M. Oberthaler, Rev. Mod. Phys. **78**, 179 (2006)
3. O. Morsch, J.H. Muller, M. Cristiani, D. Ciampini, E. Arimondo, Phys. Rev. Lett. **87**, 140402 (2001)

4. M. Cristiani, O. Morsch, J.H. Muller, D. Ciampini, E. Arimondo, Phys. Rev. A **65**, 063612 (2002)
5. L. Fallani, F.S. Cataliotti, J. Catani, C. Fort, M. Modugno, M. Zawada, M. Inguscio, Phys. Rev. Lett. **91**, 240405 (2005)
6. B. Eiermann, Th. Anker, M. Albiez, M. Taglieber, P. Treutlein, K.-P. Marzlin, M.K. Oberthaler, Phys. Rev. Lett. **92**, 230401 (2004)
7. W. Chen, D.L. Mills, Phys. Rev. Lett. **58**, 160 (1987); W. Chen, D.L. Mills, Phys. Rev. B **36**, 6299 (1987)
8. N. Broderick, C.M. Sterke, Phys. Rev. E **51**, 4978 (1995); N. Broderick, C.M. Sterke, Phys. Rev. E **58**, 7941 (1998)
9. C.M. Sterke, J.E. Sipe, *Progress in Optics XXXIII*, edited by E. Wolf (Elsevier, Amsterdam, 1994), Chap. III
10. A.B. Aceves, S. Wabnitz, Phys. Lett. A **141**, 37 (1989)
11. J. Feng, F.K. Kneubühl, IEEE J. Quantum Electron. **29**, 590 (1993)
12. D.L. Mills, S.E. Trullinger, Phys. Rev. B **36**, 947 (1987)
13. C.M. Sterke, J.E. Sipe, Phys. Rev. A **38**, 5149 (1988); C.M. Sterke, J.E. Sipe, Phys. Rev. A **39**, 5163 (1989)
14. V.V. Knontop, M. Salerno, Phys. Rev. A **65** 021602 (2002)
15. O. Zobay, S. Pötting, P. Meystre, E.M. Wright, Phys. Rev. A **59**, 643 (1999)
16. P.J.Y. Louis, E.A. Ostrovskaya, Yu.S. Kivshar, Phys. Rev. A **71**, 023612 (2005)
17. E.A. Ostrovskaya, Yu.S. Kivshar, Phys. Rev. Lett. **90**, 160407 (2003)
18. P.J.Y. Louis, E.A. Ostrovskaya, C.M. Savage, Yu.S. Kivshar, Phys. Rev. A **67**, 013602 (2003)
19. Yu.S. Kivshar, S.A. Gredeskul, A. Snchez, L. Vzquez, Phys. Rev. Lett. **64**, 1693 (1990)
20. S.A. Gredeskul, Yu.S. Kivshar, K. Maslov, A. Snchez, L. Vzquez, Phys. Rev. A **45**, 8867 (1992)
21. N. Bilas, N. Pavloff, Phys. Rev. Lett. **95**, 130403 (2005)
22. C. Farrell, U. Leonhardt, J. Opt. B: Quant. Semiclass. Opt. **7**, 1 (2005)
23. D.S. Petrov, D.M. Gangardt, G.V. Shlyapnikov, J. Phys. IV **116**, 5 (2004)
24. V.A. Brazhnyi, V.V. Konotop, Mod. Phys. Lett. B **18**, 627 (2004)
25. Here the dimensionless wavevector value ($k_B = 0.5$) is determined by the rescaling form of the GPE
26. For convenience, in the following we still use the variable x and t to represent the dimensionless space and time coordinates
27. A.B. Aceves, J.V. Moloney, A.C. Newell, Phys. Rev. A **39**, 1809 (1989)
28. Since for strict GS solutions, the effective position x_s is same to the central position of GS, the variable x_s can be used to represent the central position of GS
29. If the distribution $\rho(x_i)$ of the random numeber x_i are known. For $y = x_1 + x_2 + x_3 + ... + x_n$, the disribution of y is $\rho(y) = \int_{-\infty}^{+\infty} \rho(x_1) \cdots \rho(x_i) \cdots \rho(x_{n-1}) \rho(y - \sum_{i=1}^{n-1} x_i) dx_1 \cdots dx_{n-1}$
30. Here we should point out that the integration of the denominator in equation (33) tends to be infinite if the case that $C_u W \gamma_u \geq U_c$ is included. To keep the physical meaning of the ensemble-average velocity, we only consider the case that $C_u W \gamma_u < U_c$ in the integration